Enhanced Ion Utilization Efficiency Using an Electrodynamic Ion Funnel Trap as an Injection Mechanism for Ion Mobility Spectrometry

Brian H. Clowers, **Yehia Ibrahim**, **David C. Prior**, **William F. Danielson III**, **Mikhail Belov**[*], and **Richard D. Smith**
Biological Sciences Division, Pacific Northwest National Laboratory, P.O. Box 999, Richland, WA 99352

Abstract

Conventional ion mobility spectrometers that sample ion packets from continuous sources have traditionally been constrained by an inherently low duty cycle. As such, ion utilization efficiencies have been limited to <1% in order to maintain instrumental resolving power. Using a modified electrodynamic ion funnel, we demonstrated the ability to accumulate, store, and eject ions in conjunction with ion mobility spectrometry (IMS), which elevated the charge density of the ion packets ejected from the ion funnel trap (IFT) and provided a considerable increase in the overall ion utilization efficiency of the IMS instrument. A 7-fold increase in signal intensity was revealed by comparing continuous ion beam current with the amplitude of the pulsed ion current in IFT-IMS experiments using a Faraday plate. Additionally, we describe the IFT operating characteristics using a time-of-flight mass spectrometer attached to the IMS drift tube.

Keywords

Ion mobility spectrometry; time-of-flight mass spectrometry; ion funnel; ion trapping

INTRODUCTION

In contrast to scanning gas-phase ion mobility spectrometry (IMS), such as field asymmetric ion mobility spectrometry (FAIMS)[1] and differential mobility spectrometry (DMS),[2,3] broadband IMS experiments are initiated by transmitting a discrete packet of ions into a drift tube that contains a homogeneous buffer gas and uniform electric field.[4] Traditionally, this task has been accomplished either by using pulsed ionization sources, such as matrix-assisted laser desorption ionization (MALDI),[5] or by sampling from continuous ion sources produced by radioactive[4] or electrospray ionization (ESI).[6, 7] Because multiple IMS experiments are often averaged to improve signal-to-noise ratio (SNR) and analytical confidence, it is paramount that the spatial and temporal distributions of each ion packet be highly reproducible.

The challenge of reproducibly generating an ion packet using pulsed ionization techniques is largely dependent on ion source stability. For continuous ion sources, the fidelity of the ion packets injected is not only sensitive to fluctuations in the ion beam intensity, but also to the mechanism of injection. Commonly, ion beam modulation has been accomplished using either

[*]Corresponding author
Address reprint request to: Mikhail Belov, mikhail.belov@pnl.gov, Pacific Northwest National Laboratory, P.O. Box 999/ MS K8-98, Richland, WA 99352

Tyndall[8] or Bradbury-Nielsen (BN)[9] ion gates. While fundamentally different in physical construction, both of these ion gates influence ion transmission by creating electric fields orthogonal to the drift tube axis, thereby diverting ions prior to ion mobility separation. A more recent alternative to electronic ion gate approaches builds upon the concept of introducing discrete ion packets and uses a mechanical chopper to transmit ions and initiate the IMS signal acquisition.[10]

Because the temporal spread of ions in IMS is governed by the respective contributions of ion gate pulse width, thermal diffusion, and space charge effects, maximum instrumental resolving power is attained by minimizing the gate pulse width.[11, 12] However, in practice excessively short ion gate pulse widths adversely affect signal intensities, and force a compromise between IMS resolving power and sensitivity. This balance is usually found when the ion gate pulse width is 0.1-1% of the total duration of the IMS experiment. That is, if a single IMS experiment requires 25 ms for all of the sampled ions to reach the detector, then the ion gate pulse width would typically be ~200 μs in duration. An unfortunate consequence of this experimental configuration is that of the ions generated by the continuous source > 99% are lost during the remaining 24.8 ms of the IMS experiment. Such low levels of ion utilization efficiency are a direct result of the low duty cycle of the traditional IMS analysis.

A number of experimental approaches have been developed to improve the poor duty cycle of signal averaged IMS. Although pulsed ionization techniques such as MALDI maximize ion utilization by synchronizing ion production and gating, higher signal stability is attained by using continuous ions sources such as ESI. Multiplexing techniques such as Fourier,[13, 14] Hadamard,[15, 16] and phase resolved ion gating[17] have also been employed to improve IMS duty cycle and overall ion utilization; however, transformation artifacts still prevent these methods from fully achieving the levels of throughput predicted by the Fellgett advantage.[18] Perhaps the most logical extension of existing technologies is the integration of ion trapping with IMS to maximize the effective duty cycle. Ion trapping is directly compatible with the traditional signal averaging IMS experiment and has been shown to augment multiplexing approaches.[19]

The concept of ion accumulation and IMS injection using static DC fields was first demonstrated by Blanchard and was achieved by adjusting the relative potentials of drift rings located towards the entrance of an ion mobility drift cell.[20, 21] Characterization of these "ion wells" or field gradient ion barriers (FGIB) indicated that without a mechanism to confine ions in the region immediately preceding the ion gate, the accumulation of ion species was dynamic and dependent upon the mobility of each ion population.[21] Additional examination of this ion trapping technique illustrated relatively broad injection pulses and a limited range of ion accumulation to a maximum of ~10 ms.[21] In a separate detailed assessment of the characteristics influencing ion mobility performance, Eiceman *et al.* demonstrated a refined example of increasing the local concentration of ions using DC fields produced by a dual grid ion gate.[22] Their results illustrated the ability to increase ion cloud charge density in the region immediately preceding the ion gate; however, the capacity and dynamic range of this configuration were not reported.

The benefits of incorporating ion accumulation using a three dimensional ion trap were demonstrated by both Hoaglund *et al.* and Creaser *et al.*[23, 24] These groups showed an increase in recorded ion signals as a result of collecting ions during the course of a single IMS analysis. Further development of this concept exploited the higher charge capacity of an RF-only octapole and its use as an ion injection device.[25] Both the Paul and linear ion trap configurations significantly improve the overall ion utilization efficiency of the IMS experiment; however, since the pressure within the ion trap is directly proportional to the number density of neutrals, and the concentration of neutrals greatly influence the efficiency of ion trapping, lower

pressures can adversely affect the sensitivity of an ion trap-IMS instrument. The narrow range of drift tube pressures compatible with efficient ion trapping confine this approach to a limited range of measurement conditions.

Our laboratory has recently reported the concept of accumulating ions in an electrodynamic ion funnel prior to initiating an IMS analysis.[26, 27] While ion funnel trapping technology with IMS had been previously demonstrated,[28] the ion funnel trap (IFT) configuration reported by Tang *et al.*[26] enabled accumulation and storage of ions in a significantly larger volume at operating pressures of several Torr.[27] In its initial implementation, the IFT employed an "hourglass" design that allowed ions to accumulate towards the IFT exit by using a combination of a linear DC field gradient, RF effective potential well, and a single ion grid. Although this design achieved ion trapping, the dynamic range, ion ejection efficiency, and the overall trap capacity were limited due the configuration of the trapping elements. Improvements to ion transmission through an mobility drift tube were achieved for the continuous mode (i.e., no IMS separation) by combining electrodynamic ion funnels with the IMS drift tube.[26] More recently, our laboratory demonstrated the use of a novel IFT design operated at 1 Torr in combination with a time-of-flight (TOF) mass spectrometer equipped with analog-to-digital converter (ADC) detection.[29] The results showed that improvements in ion packet charge density were accompanied by 10- to 30-fold gains in SNR with respect to signals obtained using the same instrument operating in the continuous mode.

In this work we have further refined the electrodynamic ion funnel trap design and optimized it for operation at higher pressures. The resulting configuration achieves a 10-fold increase in IMS-TOF sensitivity compared to the previous configuration, and significantly enhances the ion utilization efficiency of the IMS analysis.[21]

EXPERIMENTAL

Characterization of the IFT was conducted using two modes of detection: 1) IMS-only using a Faraday plate as a charge collector and 2) a commercial TOF instrument interfaced to a custom built IMS drift cell.

ESI Source

The ESI source consisted of a chemically etched, 20-μm i.d. emitter[30] connected to a transfer capillary (150 μm, Polymicro Technologies, Phoenix, AZ) using a zero-dead volume stainless steel union (Valco Instrument Co. Inc., Houston, TX). Sample solutions were infused using a syringe pump (Harvard Apparatus, Holliston, MA) at a flow rate of 300 nL/min. The high voltage used to sustain the electrospray was applied through the stainless steel union by a current-limited 4-channel power supply (Ultravolt, Ronkonkoma, NY) and held ~2400 V above the heated capillary inlet (150 °C). The electrospray-generated ion plume was sampled using a 64-mm long transfer capillary with an inner diameter of 0.43 mm. The potential applied to the heated transfer capillary was 210 V higher than the ion mobility drift tube voltage.

Ion Funnel Trap

The IFT was comprised of 5 regions that encompassed 75 brass electrodes. Ions were confined radially with an RF field and directed towards the IMS drift cell using a DC gradient. The effective potential used to confine ions was generated by applying RF potentials 180° out of phase to a pair of independent capacitor networks, one connected to the even numbered electrodes and the other to the odd numbered electrode set. A custom built drive generated an RF field at a frequency of 520 kHz and amplitude of 125 V_{p-p}. The DC field gradient used to drive ions through the apparatus was established using a separate resistor series that spanned the length of the IFT and connected to a 9-channel power supply (Spectrum Solutions, Inc.,

Russellton, PA). The DC electric field within the IFT was ~25 V/cm, except for the ion trapping region, which was held at ~1 V/cm.

In Figure 1a, region 1 of the IFT is characterized by a series of concentric electrodes with an inner diameter of 24 mm to guide ions into the converging region 2. A jet disruptor[31] located within the first region is used to minimize adverse affects of gas flow on ion accumulation. Once through the converging region, ions enter the trapping chamber, which contains regions 3-5 of the IFT. These regions are separated by three high-transmission nickel trapping grids (20 lines per inch; Precision E-forming, LLC, Cortland, NY), labeled as "entrance grid," "trapping grid," and "exit grid" in Figure 1a. Region 3 is comprised of a series of rings that expand in diameter from 3 mm to 18.9 mm at the IFT entrance grid. Region 4 in which ions are trapped and stored between ion gate releases consists of 10 electrodes with an inner diameter of 18.9 mm. Region 5 of the IFT incorporates converging electrodes that lead to the conductance limit between the IFT and the beginning of the ion mobility drift cell.

In order to control of the DC gradients in different regions of the ion trap, five DC connections to the resistor chain were made. The first and fifth connections were made to the entrance and exiting plates of the IFT, respectively, and the remaining three connections were made through 100 kΩ resistors to electrodes located directly adjacent to the trapping region. Connections to the electrodes surrounding the trapping region (labeled "Trap Gradient Controls" in Figure 1a) allowed adjustment of the DC gradient within the trapping region and the ejection gradient control generated the electric field guiding the ions to the ion funnel exit.

IFT performance was evaluated for both "continuous" and "trapping" modes of operation. Continuous mode refers to the IFT setting used to transmit the ion current generated by the continuous electrospray ionization without interference from the electrostatic grids within the trapping region. By setting the potential of the DC-only grids to the values equal to those of the uniform DC gradient, this mode is directly analogous to operating the system as a traditional electrodynamic ion funnel.[32, 33] Trapping mode refers to the set of conditions in which ions are accumulated within the trapping region of the ion funnel followed by a release event used to initiate the IMS analysis. The complete IFT ion gating cycle consisted of three distinct events: 1) injection and accumulation of ions, 2) ion storage, and 3) ion ejection.

Ions were accumulated within the ion funnel trap by raising and lowering the potentials on the three grids surrounding region 4 of Figure 1a in accordance with the voltage profiles shown in Figure 2a. Briefly, ions were injected into the ion trapping region by lowering the potential of the entrance grid from 80 V to 66 V, where they were radially confined by the RF potential and the mild repelling potentials applied to the trapping (61.5 V) and exit grids (68 V). After a user-defined accumulation period, the entrance gate was restored to 80 V and the experiment entered the storage phase. During both the accumulation and storage events, the exit grid was held at 68 V. The trapping and exit grids were simultaneously ramped to 51 and 49 V, respectively, to eject ions. The experimental sequence detailing these events is shown in Figure 2b. The key aspect of the IFT performance described herein is the configuration of the trapping region. Throughout the entire trapping and ejection cycle, the electric field gradient within region 3 (Figure 1a) was held at approximately 1 V/cm by applying the appropriate potentials, in this case 61 V and 60 V, respectively, to the trapping gradient controls in Figure 1a.

Ion Mobility-Quadrupole-Time of Flight Mass Spectrometer

Based on the modular drift tube design described previously,[26] the current ion mobility system was comprised of four units, each of which contained 21, 0.5-mm thick copper drift rings (80 mm o.d. × 55 mm i.d.) separated by ~10 mm Teflon spacers and connected in series with 1 MΩ high precision resistors. High voltage for the ion mobility drift cell was supplied by the same 4-channel power supply used to drive the ESI source. An 80-mm long conventional ion

funnel located at the terminus of the ion mobility drift cell was used to re-focus the disperse ion clouds that exited the IMS drift cell. The inner diameters of the ring electrodes (0.5 mm thick separated by 0.5 mm Teflon sheets) decreased linearly from 51 mm to 2.5 mm at the conductance limit, which was held at 35 V. Custom built power supplies were used to apply RF and DC voltages across the brass electrodes of the rear ion funnel. The peak-to-peak RF voltage was 115 V at a frequency of 500 kHz, and the DC electric field gradient for all experiments was adjusted to match the electric field within the IMS drift cell. The pressures (2-4 Torr) inside the IFT and ion mobility drift cell were monitored using a capacitance manometer (MKS Instruments, Willmington, MA) and regulated using a leak valve that passed dry, high purity nitrogen into the drift chamber. To maintain a buffer gas flow counter to the direction of ion velocity, the pressure in the drift cell was maintained ~30 mTorr higher than the IFT.

When conducting ion current measurements, a shielded Faraday plate was placed immediately following the conductance limit of the rear ion funnel. Ion signals were amplified using a Keithley 427 current amplifier (Keithley Instruments, Inc., Cleveland, OH) and data were recorded using a TDS-784C oscilloscope (Tektronix, Richardson, TX). For experiments employing a TOF mass spectrometer as a detector, a segmented quadrupole that consists of two 11 mm sections following the conductance limit of the rear ion funnel served to optimize ion transmission through a 2.5 mm conductance limit (~15 V). The two sections of this quadrupole were biased to 30 V and 22 V, with an RF potential of 200 V_{p-p} at a frequency of 700 kHz. The chamber between the IMS cell and quadrupole time-of-flight (Q-TOF) mass spectrometer was evacuated using a mechanical pump (Alcatel 2033) to a pressure of ~300 mTorr. Once into the Q_0 or collisional quadrupole of the modified commercial Q-TOF (MDS Sciex, Q-Star Pulsar, Concord, Canada), the ions were guided into the pulsing region of the Q-TOF operated at ~7 kHz, which spans a mass range of 50-2000 *m/z*. The ion optics of the Q-TOF system were optimized to maximize ion transmission and signal intensity while minimizing the ion transit time to the detector.

Data were recorded using an Ortec-9353 10 GHz time-to-digital converter (TDC) (Ortec, Oak Ridge, TN) interfaced to a custom built software package operating under the Windows XP operating system.[26] The timing sequence of the ion mobility experiment was synchronized with the pulsing frequency of the Q-TOF and controlled using a PCI-6711 timing card (National Instruments, Austin, TX).

Chemicals and Materials

Lyophilized leucine enkephaline, kemptide, bradykinin, fibrinopeptide A, and angiotensin I were purchased from Sigma-Aldrich (St. Louis, MO) and prepared at concentrations that ranged from 1 nM to 5 μM in an electrospray solution of 1:1 water:methanol that contained 0.1% formic acid by volume. Proteolytic digestions of bovine serum albumin (BSA) (Pierce Biotechnology, Rockford, IL) were conducted using sequencing grade trypsin (Promega, Madison, WI), following previously outlined procedures.[34] Based upon the resulting protein concentrations measured using a biocinchoninic acid assay (BCA),[35] the concentrations of digested BSA used to evaluate IFT performance ranged from 1nM to 1uM, using the solvent conditions described above.

RESULTS AND DISCUSSION

Ion Funnel Trap Design

The function of the dual or Tyndall gate[8] configuration at the IFT exit was two fold. First, this configuration mitigates the influence of the high trapping potential of the exit grid on the trapped ion populations. High trapping potentials used in conjunction with a single exit grid

give rise to ion dispersion into regions of high RF field where ion discrimination and fragmentation are likely. Second, the use of the dual trapping grid allows ion density to increase in close proximity to the exit grid, which results in faster ion ejection from the IFT. These conclusions were supported by modeling ion accumulation and ejection from the IFT in both single and dual grid configurations, using SIMION 8.0 (Scientific Instrument Services, Ringoes, NJ). The 3D profiles of the full potential (i.e., a superposition of the effective and DC potentials), as well as the DC-only potential contours are shown for both the dual exit grid design (Figure 1b) and single exit gate configuration[26] (Figure 1c). The full potential distribution for the dual gate design in Figure 1b was relatively uniform along the axis throughout the ion trapping region. This uniform profile is in stark contrast to the full potential distribution for the single gate design illustrated in Figure 1c. The high trapping potential necessary to prevent ion leakage penetrates deeply into the IFT trap, which creates conditions that divert ions from the central axis of the trap and repel them from the exit. Not only does the single gate configuration reduce the overall trapping capacity of the IFT, but it also necessitates the use of longer extraction times for full ion ejection. Compared to the previous IFT design for use with IMS,[26] the dual grid configuration allowed ions to be ejected more efficiently and also allowed the ion concentration in the region directly preceding the trapping grid to be increased. Note that similar "ion bunching" phenomena[36, 37] were observed earlier in collinear laser spectroscopy experiments. We found that the specific spatial and electrical configurations of the two grids at the IFT exit enabled both effective ion accumulation and ejection.

Ion Funnel Trap Capacity and Ejection Efficiency

To explore the performance of the new IFT in conjunctions with IMS, comparisons of ion currents were made using different accumulation, storage, and ion gate pulse widths. Because ion discrimination can occur by transferring ions into a mass spectrometer, the initial evaluation of the IFT was made using a shielded Faraday plate. This method allowed for direct measurement of IFT charge capacity and overall accumulation efficiency. Under ideal conditions using a traditional BN gate, or similar method of beam modulation, the maximum recorded ion density cannot exceed the observed continuous ion current without ion gating. However, in practice, the pulsed ion current observed during IMS operation rarely reaches the levels of continuous current detected without IMS.[4, 7, 22, 38]

Figure 3a shows a comparison of the ion mobility spectra acquired using the IFT-IMS and continuous ion current (i.e., signal obtained in continuous mode) for 5 μM kemptide. These data illustrate that even for an ion gate pulse width of 100 μs, the overall signal intensity (146 pA) was greater than the continuous ion current (140 +/- 1 pA). An increase in the ion gate pulse width resulted in a significant increase in the kemptide signal amplitude. For example, using a release time of 400 μs, the signal intensity exceeded the continuous current by a factor 7

Figure 3b compares the total number of charges observed for a given IMS spectrum as a function of ion gate pulse width. The total number of charges delivered to the detector can be determined by integrating the area under each IMS spectrum acquired using the Faraday plate and dividing by the unit of elementary charge (1.602×10^{-19} C). Application of this methodology to the data shown in Figure 3a resulted in the upper most trace of Figure 3b,which corresponds to the IFT configuration that utilized the "dual trapping grid" configuration. A separate data set obtained using the previous IFT configuration and a "single trapping grid" is plotted in Figure 3b for comparison. (It should be noted that all data in Figure 3b were acquired by accumulating ions throughout the length of each IMS experiment.) The plots in Figure 3b also illustrate that the relative increases in signal intensity decreased exponentially as pulse width increased. This maximum limit reflects the charge capacity of the system, and the rate

at which the limit is reached depends on the position of the trapped ion cloud with respect to the IFT exit. More specifically, this plot validates the concept of ion bunching and indicates that the density of the ion beam is at a maximum close to the trapping and exit gates and decreases towards the entrance of the funnel. As the charge capacity of any given ion trapping system is fixed, the time needed to reach this limit is influenced by two primary factors: incoming ion beam density (related to sample concentration, ionization efficiency and inlet transfer) and trapping efficiency. For the dual trapping grid configuration, Figure 3b indicates the maximum trap capacity was slightly greater than 15 million ions, and ~350 μs was required to inject these ions into the IMS drift tube. Compared to the previous implementation of the IFT, the rate of ion accumulation and maximum trap capacity using dual trapping grids is greater by a factor of ~3. In both IFT configurations longer release times resulted in only a limited increase in the ion signal because the majority of analyte ions had already exited the IFT. An ideal experimental configuration would allow for the rapid ejection of ions to attain a constant level of signal intensity regardless of ion gate release time. In practice, the rate of evacuation from stacked ring trap such as the IFT is ion mobility dependent,[22, 39] so that higher mobility species exit the IFT faster. The presented results demonstrate the ability of the IFT to accumulate ions from a continuous source and provide an insight into the charge capacity and ejection efficiency of the IFT.

Ion Funnel Trapping Efficiency

In order to assess the ion funnel trapping efficiency and relative charge density of ejected ion populations, experiments were performed to directly compare the total ion currents generated in continuous and trapping modes of operation. Specifically, the total ion charge observed for a single IFT accumulation and release event was compared to total charge observed for an equivalent time of continuous current. This comparison is represented in Figure 4a, which graphically depicts a subset of the signals recorded by varying the accumulation time of a 1 μM leucine enkephalin sample from 1-80 ms. In all cases the ion gate release was fixed at 300 μs, while only the length of ion accumulation was varied. The hatched box labeled "expected charge" represents the total ion charge that would have been accumulated over an equivalent time had the efficiency been 100%. The ratio of these two values is the ion accumulation efficiency, which is plotted as a function of the ion accumulation time in Figure 4b.

The trapping efficiencies for a set of experiments are also shown in Figure 4b to illustrate not only the influence of accumulation time on trapping efficiency, but also the roles of sample concentration, ion charge state, and system pressure. Analyses of 5 μM kemptide and 1 μM leucine enkephalin were conducted at pressures of 2 and 4 Torr nitrogen. Accumulation times were adjusted by selecting the time at which the entrance gate permitted the continuous ion beam to enter the trapping region of the IFT (see Figures 1a and 2b). Generally, as the ion accumulation time was minimized, the greatest gains were observed for the accumulation efficiency. Including data not shown efficiencies for accumulation times less than 10 ms were > 60% and in some cases approached 100%. The primary reason for a decrease in accumulation efficiency as accumulation time increases is directly related to the charge capacity and the rate at which this limit was reached (see discussion of Figure 3). This decrease is also estimated to be a function of the axial distribution of ions within the trap. Given the previously determined charge capacity of ~15 million charges, gains in accumulation efficiency would be expected until that limit was reached. However, as the data in Figure 4b illustrate the IFT accumulation efficiency decreases logarithmically with accumulation time. These data indicate that in addition to charge capacity, ion ejection efficiency influences the observed accumulation efficiency. By increasing the length of accumulation, the axial distribution of ions within the IFT also expands. Hence, the use of a fixed ejection pulse width limits the total ejected charge for large ion populations. Extended release time may increase the overall efficiency, but at the expense of ion mobility resolution. Despite these caveats, trapping efficiencies as low as 10%

and up to 100% were achieved for the range of analytes examined with the charge collector. Even under the most unfavorable trapping conditions, an ion utilization efficiency of 10% is a significant improvement over the duty cycle of traditional IMS experiments. Figure 4b also indicates that purging the IFT after short accumulation intervals (i.e., such as with multiplexing[14]) would further increase ion utilization efficiency.

Ion Mobility Time-of-Flight Mass Spectrometry

Analyses similar to those in the charge collector experiments were performed by combining the IMS drift cell with a Q-Star TOF-MS. The added degree of selectivity provided by the *m/z* dimension further validated results observed using the charge collector. The trapping time necessary to reach the IFT charge capacity was reduced for higher analyte concentrations and deviated from linearity at ~16 ms for peptide concentrations above 100 nM. For lower peptide concentrations (5 nM) the rate at which the IFT reaches its charge capacity was significantly reduced to the point that the maximum level did not appear to be reached during the course of an IMS experiment (60 ms). These results are summarized in Figure 5, which plots the recorded intensity for a mixture of peptides at high and low analyte concentrations against the accumulation time within the IFT.

Assessing trapping efficiency using the TOF mass spectrometer required direct comparisons between the number of ion counts observed for a given *m/z* over the same length of time in the continuous and trapping modes. As observed in the charge collector experiments, higher analyte concentrations combined with extended accumulation times typically created a set of conditions in which the utility of the IFT was exhausted in a relatively short amount of time. The gains provided by the IFT were most apparent during examinations of samples that contained low concentrations of analytes. Under these circumstances, the time at which the IFT was filled to capacity approached the duration of a single IMS experiment (see Figure 5b), which in turn maximized the ion utilization and effective duty cycle. Figure 6 illustrates the ion accumulation efficiency of the IFT using the mass spectrometer as a detector for a 5 nM solution of neurotensin. Mass spectra acquired from the continuous beam were summed for the same amount of time that ions were accumulated using the IFT during the IMS-TOF experiment to accurately compare the two modes of operation. The upper-most plot in Figure 6a compares the summed isotopic distribution for neurotensin $[M+3H]^{+3}$ observed for an 8 ms IFT accumulation time and the summed *m/z* spectrum acquired for a continuous beam acquisition of equal length. Based on the total area under the individual isotopic distributions, the IFT trapping efficiency was 60% for an 8 ms accumulation and >80% for a 2 ms accumulation—a result that directly supports the charge collector measurements of trapping efficiency.

In contrast to operation in the continuous mode, ion packets are distributed based upon their mobility throughout the IMS drift tube. Consequently, a considerable number of spectra are completely void of ions when the TOF was used as the detector. In previous sections we illustrated the ability of the IFT to accumulate and introduce ion packets into the IMS drift tube that possess current densities that exceed continuous current levels. However, because a discrete counting device (i.e., time-to-digital converter, TDC) was used as the TOF recording mechanism, the *m/z* signal intensities do not accurately reflect increases in delivered charge density. The *m/z* signal intensities do, on the other hand, reflect an increase in the probability of recording an ion arrival event at the detector. This increase in the probability of ion counting for a single TOF pulse obtained in the trapping mode compared to the continuous mode is shown in Figure 7. The signal for the zoomed view of the isotopic envelope for the trypic BSA peptide KVPQVSTPTLVEVSR $[M+3H]^{+3}$ represents the probability of ion counting observed between the trapping and continuous modes of operation using 300 TOF spectra (Figure 7b). The trapping mode data (accumulation time: 16 ms) were obtained from the IMS peak

maximum. The counts per TOF pulse were obtained by dividing the total ion counts observed by the number of TOF spectra used to acquire the total signal. On average the number of ion counts observed at the maximum of an IMS peak exceeded the counts for the same m/z ratio in the continuous beam by a factor 2. While this gain in the number of ion counts per TOF pulse does not indicate the actual gains in the charge density produced by the IFT due to TDC constraints, these data do support the conclusion that increases in charge density lead to higher probabilities of detection. The actual gains obtained by combining the IFT with the IMS experiment would be best realized using an ADC device in conjunction with a TOF detector.

To examine the effect of ion funnel accumulation and storage time on more complex ion populations, the percent coverage for a tryptic digestion of BSA was determined for a range of sample concentrations. Figure 8a illustrates the characteristic sequence coverage behavior observed for two concentrations, i.e., 200 nM and 60 nM,. All peptide assignments were made using a 20 ppm window for matching the deisotoped spectrum (e.g., Figure 7a.) to a theoretical *in silico* tryptic digestion of BSA. In accord with previous observations using the IFT, the rate of signal increase at lower ion accumulation times was greater for the more concentrated BSA samples. Consequently, the number of BSA tryptic fragments also increased compared to the equivalent accumulation time using lower concentrations. The 200 nM sample of BSA reached maximum sequence coverage of ~70% for an accumulation time of 8 ms, while the 60 nM BSA sample peaked at ~65 %, which corresponds to an accumulation time of 16 ms. Given the flow rate of 300 nL/min, the total sample consumed for the two BSA digest concentrations were ~ 5 fmol and 18 fmol for the 60 nM and 200 nM samples, respectively.

Although spectral quality did not degrade at longer accumulation times, the number of confident peptide assignments was reduced compared to those at accumulation times below 16 ms. This observation was attributed to the discriminatory effects induced by exceeding the charge capacity of the IFT. For extended accumulation times, the effect of Coulombic repulsion and its influence on ion instability within the IFT create a set of conditions in which selected ion loses may occur. Discrimination of trapped ion populations is well documented in the literature,[40-42] Loss of ions when space charge capacity is exceed often occur by two primary mechanisms. The first mechanism of ion loss is related to the radial stratification of the higher m/z ion populations. As the global charge density of an ion trap increases, the radial stratification of a select m/z also increase due the repelling forces of ions occupying the center of the ion trap. If the stable radius of a specific ion population exceeds the dimensions of the trap they will be neutralized. The second mechanism related to space charge induced ion losses is related to the stability of lower m/z ion populations. Previous work has illustrated that as the ion population within a RF ion trap approaches the space charge limit the range of m/z stability also narrows with a particular emphasis on lower m/z ions. For these two reasons ion losses within the IFT may be observed when the charge capacity of the system is exceeded.

Effect of Ion Funnel Storage Time

Another feature that demonstrates the effectiveness of the IFT is its ability to store ions for extended periods of time with minimal losses. It was initially observed that changes in signal intensities were minimal mixtures of simple peptides. In order to examine the effect of IFT storage time on more complex samples the percent coverage observed for a 60 nM solution of BSA was examined by accumulating ions for 5 ms while varying ion storage time (See Figure 2 for schematic of the timing scheme). For a 5 ms accumulation time and 0 ms storage time the maximum BSA coverage was 47 +/-3 %. This value slowly decreased linearly to a minimum of 38 +/- 2 % coverage of BSA after storing the ions for 62 ms. These results demonstrate that even for complex samples, the IFT was able to store ions for up to ~60 ms with minimal loss.

CONCLUSIONS

This work demonstrates that incorporation of a dual grid gating design with an IFT can increase the effective charge capacity, ejection efficiency and ion packet charge density of the IFT. A 7-fold increase in signal was observed based on comparisons of the pulsed ion current obtained from IFT-IMS experiments with continuous ion current. Because the amplitude of ion pulses from a traditional IMS analysis rarely reaches the continuous ion current level, we estimate that the IFT allows injection of ion packets with ion densities that are an order of magnitude greater than their counterparts that use conventional IMS gating mechanisms. Additional comparisons between trapped and continuous signal levels indicated that for minimal ion accumulation times, the ion utilization efficiency of the IFT approached 100%. While these short accumulation times (<10 ms) are much less than a typical IMS scan time (~ 60 ms), such accumulation times are an ideal length for integration with other approaches, including multiplexing,[14] to enhance instrumental duty cycle. By combining the efficient ion accumulation of the IFT with techniques such as multiplexing, the traditional limitations of the IMS duty cycle can be effectively circumvented and ion utilization efficiencies of >50% realized.

References

1. Guevremont R. High-field asymmetric waveform ion mobility spectrometry: A new tool for mass spectrometry. Journal of Chromatography A 2004;1058(12):3–19. [PubMed: 15595648]

2. de la Mora JF, Ude S, Thomson BA. The potential of differential mobility analysis coupled to MS for the study of very large singly and multiply charged proteins and protein complexes in the gas phase. Biotechnol J 2006;1(9):988–97. [PubMed: 16941442]

3. Nazarov EG, Miller RA, Eiceman GA, Stone JA. Miniature differential mobility spectrometry using atmospheric pressure photoionization. Anal Chem 2006;78(13):4553–63. [PubMed: 16808465]

4. Eiceman, GA.; Karpas, Z. Ion Mobility Spectrometry. 2nd Edition. 2004. p. 368

5. Gillig KJ, Ruotolo B, Stone EG, Russell DH, Fuhrer K, Gonin M, Schultz AJ. Coupling High-Pressure MALDI with Ion Mobility/Orthogonal Time-of-Flight Mass Spectrometry. Anal. Chem 2000;72(17): 3965–3971. [PubMed: 10994952]

6. Gieniec JM,LL, Nakamae K, Gupta C, Kumar V, Dole M. Electrospray mass spectroscopy of macromolecules: Application of an ion-drift spectrometer. Biological Mass Spectrometry 1984;11(6): 259–268.

7. Wittmer D, Chen YH, Luckenbill BK, Hill HH. Electrospray Ionization Ion Mobility Spectrometry. Anal. Chem 1994;66(14):2348–2355.

8. Mason, E,A.; McDaniel, EW. Transport Properties of Ions in Gases. 2nd ed.. Wiley; New York, New York: 1988. p. 560

9. Bradbury NE, Nielsen RA. Absolute Values of the Electron Mobility in Hydrogen. Physical Review 1936;49(5):388.

10. Zhou L, Collins DC, Lee ED, Lee ML. Mechanical ion gate for electrospray-ionization ion-mobility spectrometry. Anal Bioanal Chem 2007;388(1):189–94. [PubMed: 17345070]

11. Revercomb HE, Mason EA. Theory of plasma chromatography/gaseous electrophoresis. Review. Anal. Chem 1975;47(7):970–983.

12. Siems WF, Wu C, Tarver EE, Hill HH Jr. Larsen PR, McMinn DG. Measuring the Resolving Power of Ion Mobility Spectrometers. Anal. Chem 1994;66(23):4195–4201.

13. Knorr FJ, Eatherton RL, Siems WF, Hill HH Jr. Fourier transform ion mobility spectrometry. Anal Chem 1985;57(2):402–6. [PubMed: 3977072]

14. Dietiker R, diLena F, Chen P. Fourier Transform Ion Mobility Measurement of Chain Branching in Mass-Selected, Chemically Trapped Oligomers from Methylalumoxane-Activated, Metallocene-Catalyzed Polymerization of Ethylene. J. Am. Chem. Soc 2007;129(10):2796–2802. [PubMed: 17302412]

15. Clowers BH, Siems WF, Hill HH, Massick SM. Hadamard transform ion mobility spectrometry. Anal Chem 2006;78(1):44–51. [PubMed: 16383309]

16. Szumlas AW, Ray SJ, Hieftje GM. Hadamard transform ion mobility spectrometry. Anal Chem 2006;78(13):4474–81. [PubMed: 16808456]

17. Szumlas AW, Hieftje GM. Phase-resolved detection in ion-mobility spectrometry. Analytica Chimica Acta 2006;566(1):45–54.

18. Fellgett, PB. Thesis, University of Cambridge. UK: 1951. The Multiplex Advantage.

19. Belov ME, Buschbach MA, Prior DC, Tang K, Smith RD. Multiplexed ion mobility spectrometry-orthogonal time-of-flight mass spectrometry. Anal Chem 2007;79(6):2451–62. [PubMed: 17305309]

20. Blanchard WC. Using nonlinear fields in high pressure spectrometry. International Journal of Mass Spectrometry and Ion Processes 1989;95(2):199–210.

21. Blanchard WCN,EG, Carr J, Eiceman GA. Ion Injection in a Mobility Spectrometer using Field Gradient Barriers, i.e. Ion Wells. International Journal of Ion Mobility Spectrometry 2002;5(3):15–18.

22. Eiceman GA, Nazarov EG, Rodriguez JE, Stone JA. Analysis of a drift tube at ambient pressure: Models and precise measurements in ion mobility spectrometry. Review of Scientific Instruments 2001;72(9):3610–3621.

23. Hoaglund CS, Valentine SJ, Clemmer DE. An Ion Trap Interface for ESI-Ion Mobility Experiments. Anal. Chem 1997;69(20):4156–4161.

24. Creaser CS, Benyezzar M, Griffiths JR, Stygall JW. A tandem ion trap/ion mobility spectrometer. Anal Chem 2000;72(13):2724–9. [PubMed: 10905299]

25. Myung S, Lee YJ, Moon MH, Taraszka J, Sowell R, Koeniger S, Hilderbrand AE, Valentine SJ, Cherbas L, Cherbas P, Kaufmann TC, Miller DF, Mechref Y, Novotny MV, Ewing MA, Sporleder CR, Clemmer DE. Development of high-sensitivity ion trap ion mobility spectrometry time-of-flight techniques: a high-throughput nano-LC-IMS-TOF separation of peptides arising from a Drosophila protein extract. Anal Chem 2003;75(19):5137–45. [PubMed: 14708788]

26. Tang K, Shvartsburg AA, Lee HN, Prior DC, Buschbach MA, Li F, Tolmachev AV, Anderson GA, Smith RD. High-sensitivity ion mobility spectrometry/mass spectrometry using electrodynamic ion funnel interfaces. Anal Chem 2005;77(10):3330–9. [PubMed: 15889926]

27. Baker ES, Clowers BH, Li F, Tang K, Tolmachev AV, Prior DC, Belov ME, Smith RD. Ion Mobility Spectrometry-Mass Spectrometry Performance Using Electrodynamic Ion Funnels and Elevated Drift Gas Pressures. J Am Soc Mass Spectrom. 2007

28. Wyttenbach T, Kemper PR, Bowers MT. Design of a new electrospray ion mobility mass spectrometer. International Journal of Mass Spectrometry 2001;212:13–23.

29. Ibrahim, Y. B., Mikhail; Tolmachev, Aleksey; Smith, Richard, D. Higher-Pressure Ion Funnel Trap Interface for Orthogonal Time-of-Flight Mass Spectrometry. Analytical Chemistry. 2007Accepted Manuscript, July 2007

30. Kelly RT, Page JS, Luo Q, Moore RJ, Orton DJ, Tang K, Smith RD. Chemically etched open tubular and monolithic emitters for nanoelectrospray ionization mass spectrometry. Anal Chem 2006;78(22):7796–801. [PubMed: 17105173]

31. Kim T, Tang K, Udseth HR, Smith RD. A multicapillary inlet jet disruption electrodynamic ion funnel interface for improved sensitivity using atmospheric pressure ion sources. Anal Chem 2001;73(17):4162–70. [PubMed: 11569805]

32. Belov ME, Gorshkov MV, Udseth HR, Anderson GA, Tolmachev AV, Prior DC, Harkewicz R, Smith RD. Initial implementation of an electrodynamic ion funnel with Fourier transform ion cyclotron resonance mass spectrometry. J Am Soc Mass Spectrom 2000;11(1):19–23. [PubMed: 10631660]

33. Kim T, Tolmachev AV, Harkewicz R, Prior DC, Anderson G, Udseth HR, Smith RD. Design and implementation of a new electrodynamic ion funnel. Anal Chem 2000;72(10):2247–55. [PubMed: 10845370]

34. Kinter, M,M.; Sherman, Nicholas, E. Protein Sequencing and Identification Using Tandem Mass Spectrometry. Wiley-Interscience; New York: 2000. p. 320

35. Smith PK, Krohn RI, Hermanson GT, Mallia AK, Gartner FH, Provenzano MD, Fujimoto EK, Goeke NM, Olson BJ, Klenk DC. Measurement of protein using bicinchoninic acid. Anal Biochem 1985;150 (1):76–85. [PubMed: 3843705]

36. Nieminen A, Campbell P, Billowes J, Forest DH, Griffith JA, Huikari J, Jokinen A, Moore ID, Moore R, Tungate G, Aysto J. On-line ion cooling and bunching for collinear laser spectroscopy. Phys Rev Lett 2002;88(9):094801. [PubMed: 11864015]

37. Nieminen A, Huikari J, Jokinen A, Aysto J, Campbell P, Cochrane ECA. Beam cooler for low-energy radioactive ions. Nuclear Instruments and Methods in Physics Research Section A: Accelerators, Spectrometers, Detectors and Associated Equipment 2001;469(2):244–253.

38. Wu C, Klasmeier J, Hill HH Jr. Atmospheric pressure ion mobility spectrometry of protonated and sodiated peptides. Rapid Commun Mass Spectrom 1999;13(12):1138–42. [PubMed: 10390859]

39. Luca A, Schlemmer S, Cermak I, Gerlich D. On the combination of a linear field free trap with a time-of-flight mass spectrometer. Review of Scientific Instruments 2001;72(7):2900–2908.

40. Belov ME, Nikolaev EN, Harkewicz R, Masselon CD, Alving K, Smith RD. Ion discrimination during ion accumulation in a quadrupole interface external to a Fourier transform ion cyclotron resonance mass spectrometer. International Journal of Mass Spectrometry 2001;208(13):205–225.

41. Douglas DJ, Frank AJ, Mao D. Linear ion traps in mass spectrometry. Mass Spectrom Rev 2005;24 (1):1–29. [PubMed: 15389865]

42. Tolmachev AV, Udseth HR, Smith RD. Modeling the ion density distribution in collisional cooling RF multipole ion guides. International Journal of Mass Spectrometry 2003;222:155–174.
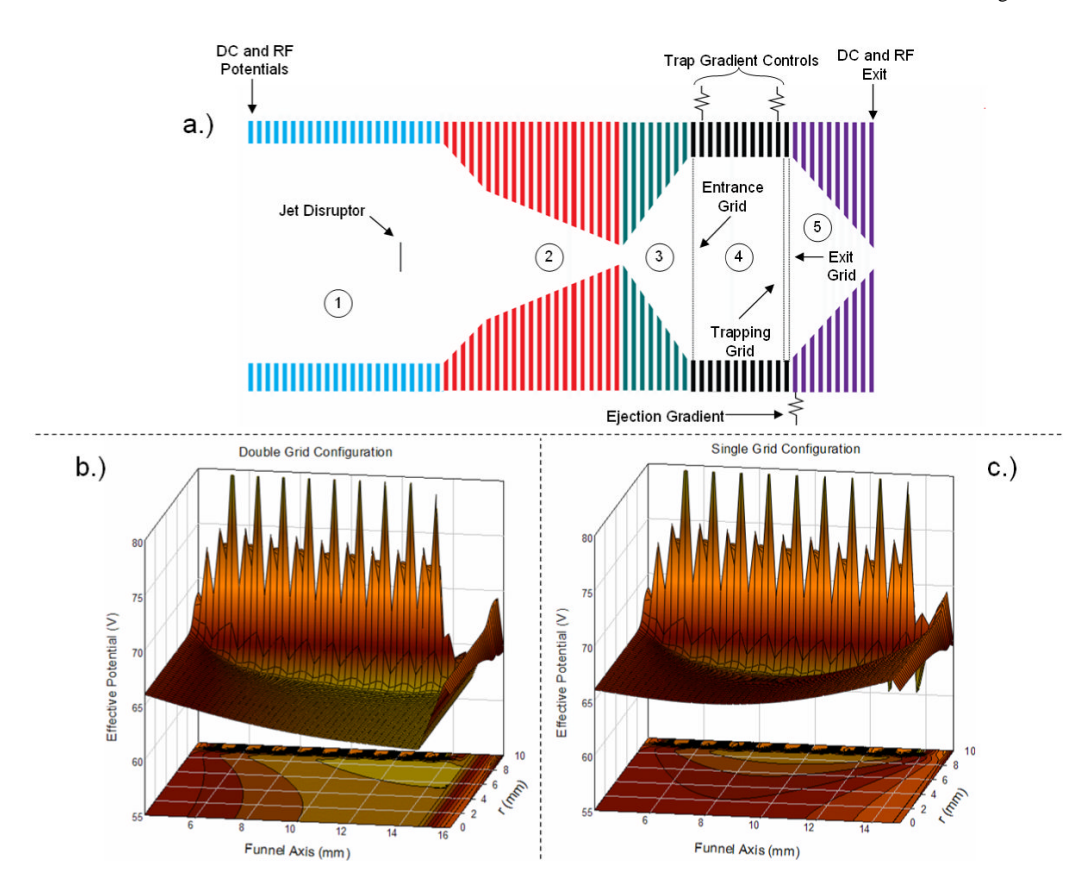
Figure 1.
(a) Annotated schematic of the ion funnel trap consisting of five distinct regions that: 1) accept the rapidly expanding free jet of ions, 2) focus ions entering the chamber that houses the next three regions that 3) guide ions into 4) the ion trapping region and 5) the final converging region and funnel exit. Regions 3, 4, and 5 are separated by a series of DC-only grids used to trap and eject the ions accumulated in region 4. The 3D full potentials and equipotential DC field lines produced by using single (b) and double exit grid (c) configurations. Note that when the potentials are appropriately adjusted in (b), the relatively homogenous field allows ions to occupy the trap region immediately preceding the ion gate. Arrangement in (c) is characterized by increased radial dispersive forces and deeper penetration of the exit grid potential into the IFT.
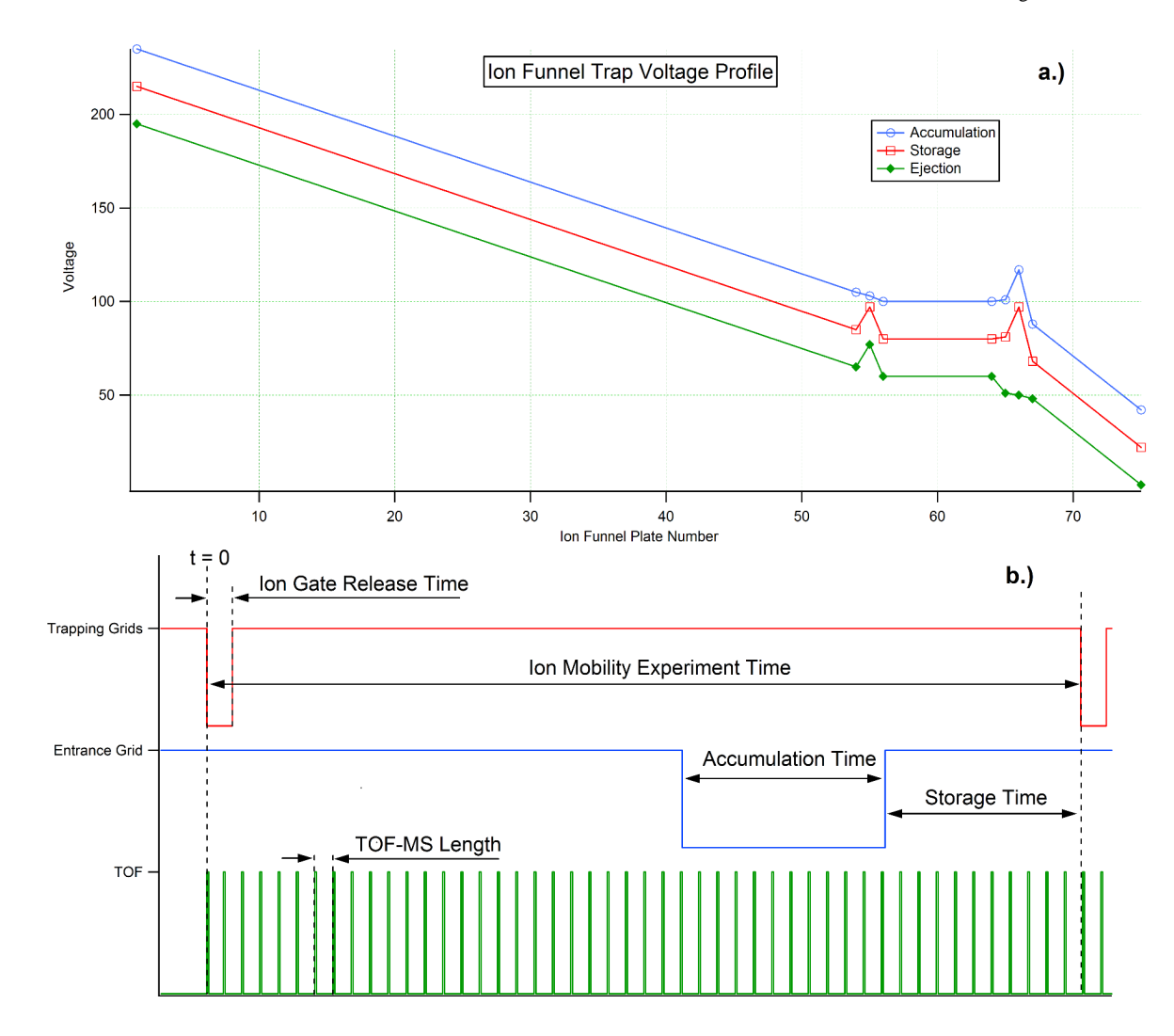
Figure 2.
a.) The ion funnel trap voltage profiles used to accumulate, store, and eject ions into the IMS drift cell. The upper and lower traces were offset from the middle profile for clarity. b.) Outline of the experimental timing sequence used with the IFT.
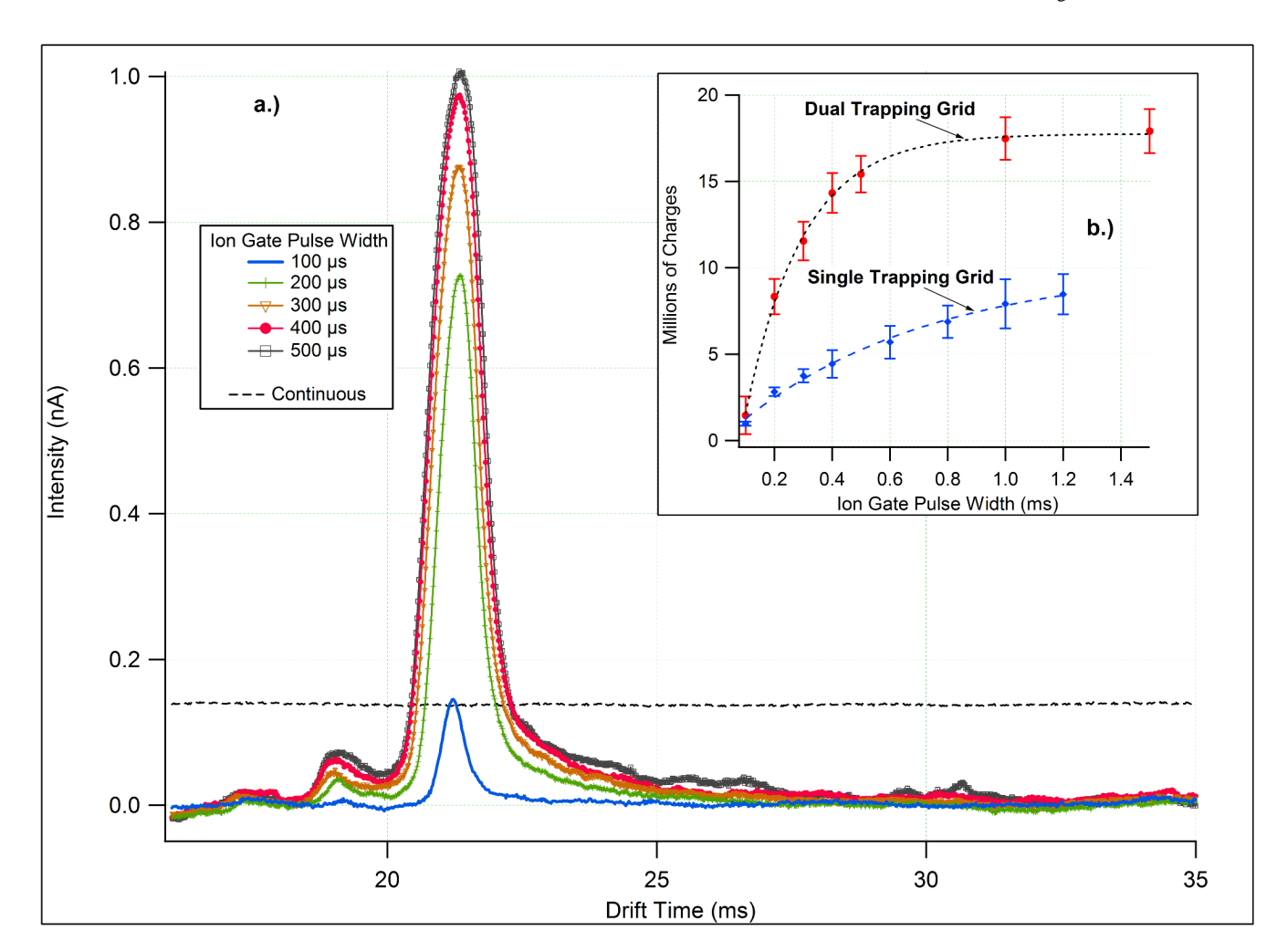
Figure 3.
Ion mobility peaks recorded for 5 µM kemptide using a shielded Faraday plate as a function of ion gate pulse width. The dashed horizontal line represents the continuous levels of current observed for the same solution without ion trapping. These data illustrate the ability of the IFT to increase ion packet charge density beyond that of a continuous ion beam. The inset plot illustrates the efficiency of ion packet ejection from IFT as a function of gate pulse width.
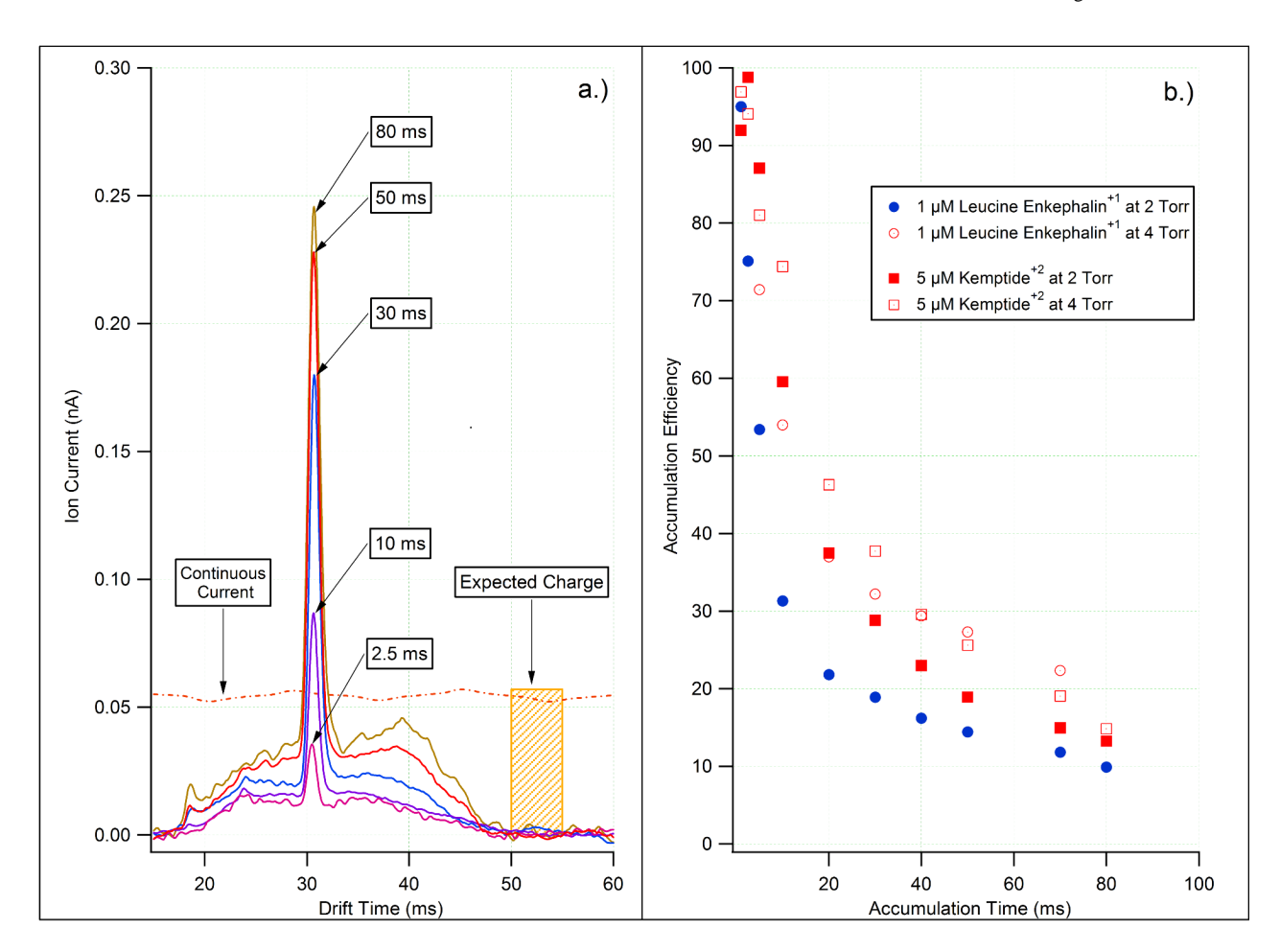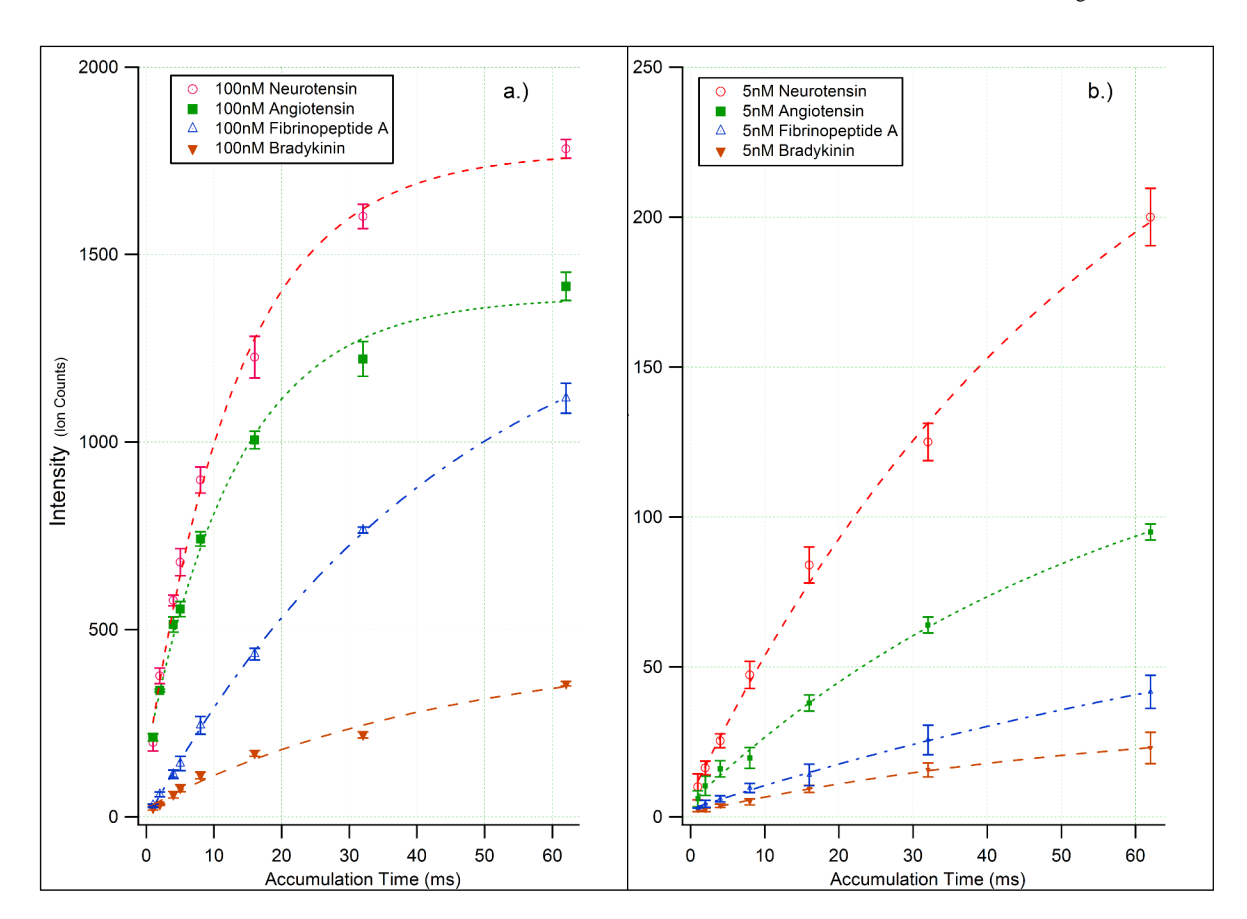
Figure 4.
a). IMS traces acquired for a 1 µM solution of leucine enkephalin using various IFT storage times acquired using a shielded Faraday plate. The continuous level of current measured for this solution is shown as a dotted line. The hatched box located at ~50 ms represents a hypothetical area under the continuous current that can be used to assess the trapping efficiency of the IFT. b) By dividing the area observed for an IMS spectrum acquired for a given trapping time by the continuous levels of current for an equal amount of time (hatched box) the efficiency of trapping was deduced for leucine enkephalin and kemptide.

Figure 5.
Signal intensities of neurotensin, angiotensin, fibrinopeptide A, and bradykinin at different concentrations plotted against accumulation time within the IFT. These data, supported by charge collector measurements, indicate that higher sample concentrations result in non-linear rates of IFT accumulation.
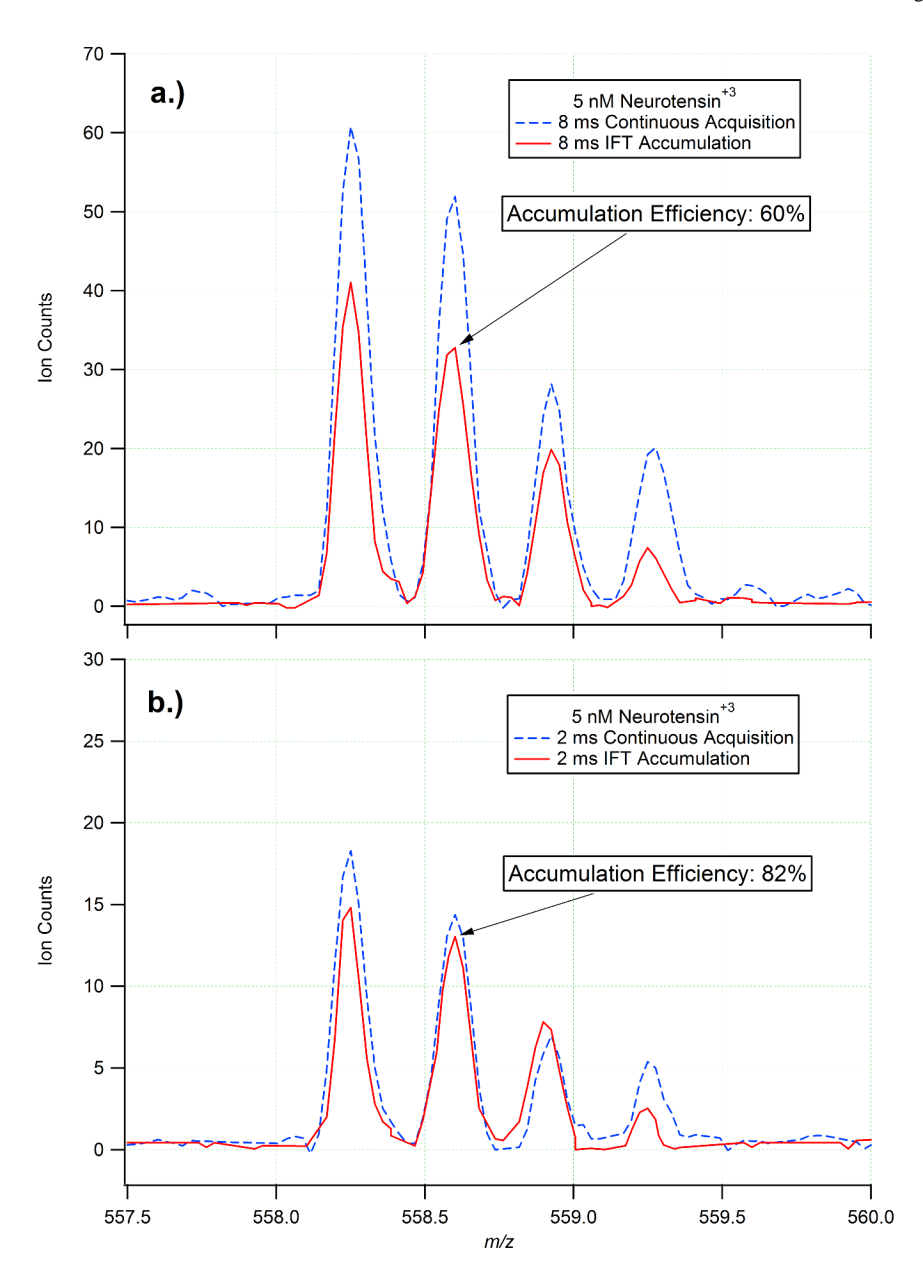
Figure 6.
To illustrate the efficiency of IFT accumulation, the relative areas for the isotopic distribution of neurotensin $[M+3H]^{+3}$ are compared for accumulation times of 8 and 2 ms (a. and b. respectively). These data show that for shorter accumulation times trapping efficiencies are increased.
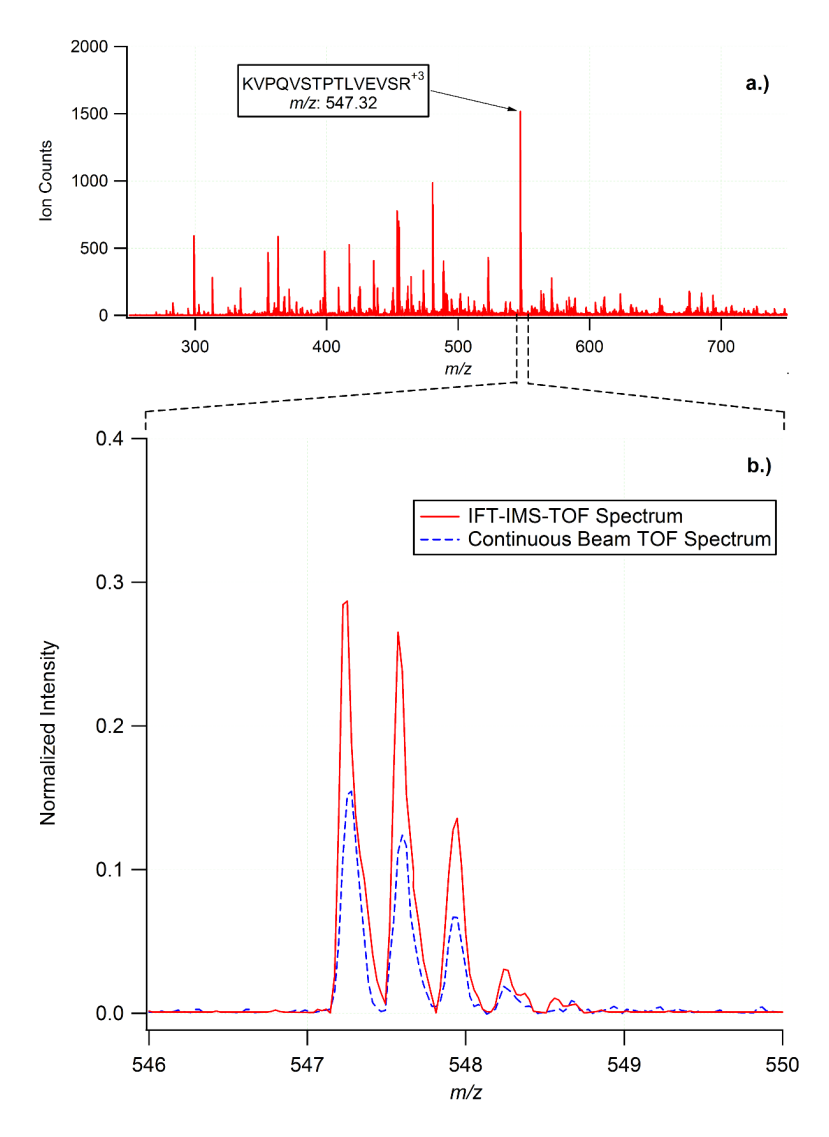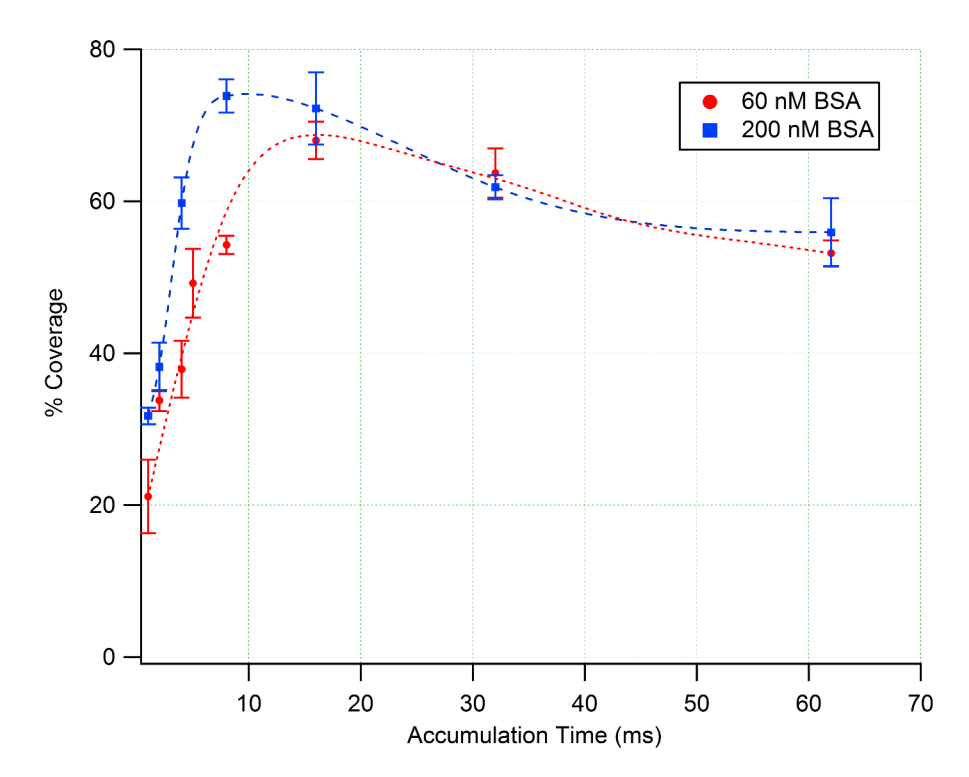
Figure 7.
a.) Sum of mass spectra acquired in 18 seconds for a 200 nM BSA digest (~ 18 fmol) and summed across all drift times. b.) Isotopic envelope of the BSA tryptic peptide KVPQVSTPTLVEVSR^{+3}. The mass spectra shown in b) reflect the signal that was obtained for a single TOF push in the IFT-IMS-TOF and continuous beam experiments. The spectrum corresponding to the IFT-IMS-TOF experiment was taken from the maximum of the IMS peak corresponding to the selected peptide.

Figure 8.
The percent sequence coverage of BSA versus IFT accumulation time. For the higher concentration of BSA the maximum percent coverage was obtained after accumulating ions for 8 ms. The BSA coverage returns to 55 % when extended accumulation times were used and demonstrate the adverse affects of exceeding the charge capacity of the IFT.